A Phase-Domain Readout Circuit for a CMOS-Compatible Hot-Wire CO_2 Sensor

Cai, Zeyu; van Veldhoven, Robert; Suy, Hilco; de Graaf, Ger; Makinwa, Kofi A. A.; Pertijs, Michiel A. P.

DOI
10.1109/JSSC.2018.2866374

Publication date
2018

Document Version
Final published version

Published in
IEEE Journal of Solid-State Circuits

A Phase-Domain Readout Circuit for a CMOS-Compatible Hot-Wire CO_2 Sensor

Zeyu Cai, *Member, IEEE*, Robert van Veldhoven, *Senior Member, IEEE*, Hilco Suy, Ger de Graaf, Kofi A. A. Makinwa, *Fellow, IEEE*, and Michiel A. P. Pertijs, *Senior Member, IEEE*

***Abstract*— This paper presents a readout circuit for a carbon dioxide (CO_2) sensor that measures the CO_2-dependent thermal time constant of a hot-wire transducer. The readout circuit periodically heats up the transducer and uses a phase-domain $\Delta\Sigma$ modulator to digitize the phase shift of the resulting temperature transients. A single resistive transducer is used both as a heater and as a temperature sensor, thus greatly simplifying its fabrication. To extract the transducer's resistance, and hence its temperature, in the presence of large heating currents, a pair of transducers is configured as a differentially driven bridge. The transducers and the readout circuit have been implemented in a standard 0.16-μm CMOS technology, with an active area of 0.3 and 3.14 mm^2, respectively. The sensor consumes 6.8 mW from a 1.8-V supply, of which 6.3 mW is dissipated in the transducers. A resolution of 94-ppm CO_2 is achieved in a 1.8-s measurement time, which corresponds to an energy consumption of 12 mJ per measurement, >10× less than prior CO_2 sensors in CMOS technology.**

***Index Terms*— Carbon dioxide (CO_2) sensor, CMOS compatible, delta–sigma modulator, phase-domain readout, resistive sensor, thermal conductivity (TC).**

I. Introduction

CARBON dioxide (CO_2) measurement is an important function in home and building automation [1]–[4]. CO_2 concentration is an indicator of indoor air quality. It can be used to estimate the occupancy of a building and correlates with the degree of comfort experienced by the occupants [1], [2]. Adverse effects on human productivity have been reported for average CO_2 concentrations as low as 1000 ppm [2], [3]. Regulations limit indoor CO_2 concentration to 5000 ppm [2]. Applications such as demand-controlled ventilation in energy-efficient buildings [4] require low-cost, low-power, and miniaturized CO_2 sensors that are compatible with this concentration range. Optical CO_2 sensors based on the absorption of non-dispersive infrared (NDIR) light can achieve resolutions well below 100 ppm, suitable for indoor CO_2 sensing. However, they are quite expensive, difficult to miniaturize (large sensing length), and power hungry (>100 mW) [5]–[7]. Efforts have been made to realize compact MEMS-based infrared emitters in SOI technology [8]–[10]; however, the resulting resolution is inferior to that achieved by conventional microbulb-based IR emitters [8]. A fiber-optic CO_2 sensor operating in the near-IR spectrum has been proposed in [11] to reduce the sensing length to 8 cm. Sensors based on other sensing methods, such as electrochemical methods or solid electrolytes, have also been proposed in recent years [12], [13]. They are generally less expensive than optical sensors, but their accuracy and long-term stability still need further investigation.

Thermal-conductivity (TC)-based sensors, due to their CMOS compatibility, are an attractive alternative [14]–[18]. They exploit the fact that the TC of CO_2 is lower than that of the other constituents of air, so that CO_2 concentration can be indirectly measured via the heat loss of a suspended heated wire to ambient. Although TC-based CO_2 sensors have an inherently poor selectivity, this is not a problem in indoor-air monitoring, since exhalation of CO_2 is then the main cause of changes in air composition [19]. Furthermore, cross-sensitivities to temperature, humidity, and pressure can be compensated for by integrating additional sensors with the CO_2 sensor. However, compared to TC-based sensors for gases like helium or hydrogen [20], [21], the sensitivity of TC-based CO_2 sensors is typically rather low due to the relatively small difference in the TCs of CO_2 and air. In fact, a 1-ppm change in CO_2 concentration will only result in a 0.37-ppm change in the TC of air. In practice, the actual sensitivity may be even lower, due to heat loss to the substrate. In [14], a TC transducer fabricated in CMOS technology only achieved a sensitivity of 0.25 ppm per ppm CO_2.

To measure TC accurately, a steady-state approach is usually employed, in which the power dissipation of a transducer is maintained at a well-defined level, and the resulting temperature rise is measured [15]–[17]. To relax the requirements on the stability of the transducer's power dissipation, Cai *et al.* [14] propose a ratiometric approach, in which the temperature and power dissipation of CO_2-sensing and reference transducers are measured, and then used to calculate a CO_2-dependent TC ratio. This approach successfully avoids the need for a stable power reference. However, the required

Manuscript received March 24, 2018; revised June 16, 2018 and July 31, 2018; accepted August 9, 2018. Date of publication September 5, 2018; date of current version October 22, 2018. This paper was approved by Associate Editor Dennis Sylvester. This work was supported in part by NXP Semiconductors, The Netherlands, and in part by ams AG, The Netherlands. *(Corresponding author: Zeyu Cai.)*

Z. Cai is with the Electronic Instrumentation Laboratory, Delft University of Technology, 2628 CD Delft, The Netherlands, and also with NXP Semiconductors, 5656 AE Eindhoven, The Netherlands (e-mail: zeyu.cai@nxp.com).

R. van Veldhoven is with NXP Semiconductors, 5656 AE Eindhoven, The Netherlands.

H. Suy is with ams AG, 5656 AE Eindhoven, The Netherlands.

G. de Graaf, K. A. A. Makinwa, and M. A. P. Pertijs are with the Electronic Instrumentation Laboratory, Delft University of Technology, 2628 CD Delft, The Netherlands (e-mail: m.a.p.pertijs@tudelft.nl).

Color versions of one or more of the figures in this paper are available online at http://ieeexplore.ieee.org.

Digital Object Identifier 10.1109/JSSC.2018.2866374

CO_2-insensitive reference transducers require capping, which complicates the packaging procedure. Moreover, the implementation in [14] uses switched-capacitor (SC) circuits to sample the voltage drop across the transducer resistance, causing the resulting resolution to be limited by kT/C noise. As a result, a high degree of oversampling is needed to reach a resolution of 200 ppm, translating into a relatively long conversion time of 30 s, and a correspondingly high energy consumption of about 340 mJ per measurement.

As an alternative to a steady-state measurement, TC can also be derived from a transient measurement of the transducer's thermal time constant τ_{th}, i.e., the product of its thermal capacitance (C_{th}) and its thermal resistance to ambient (R_{th}), since this also depends on the TC of the surrounding air [15]–[17]. This approach has the important advantage that the measurement of τ_{th} relies on a time reference, and hence the absolute temperature and power levels do not need to be accurately stabilized or measured. In prior work, τ_{th} was determined by periodically generating heat pulses in a resistive transducer, and then measuring the phase shift of the temperature transients with a separate temperature sensor: either a similar transducer [16] or a thermopile [24], [25]. In these designs, the heating and sensing elements are separate devices, and hence the thermal signal to be sensed is naturally separated from the electrical driving signal, which simplifies the process of signal conditioning. However, this inevitably results in a more complex fabrication process, in contrast with the simple CMOS-compatible single-wire transducers used in [14].

In contrast with earlier TC sensors based on transient measurements [16], [24], we present a readout circuit that allows the heating and temperature-sensing functions to be combined in a single resistive transducer [26]. This greatly simplifies fabrication, since only a single extra etch step is required to realize a tungsten hot-wire transducer in the via layer of a standard CMOS process [14]. The readout circuit is based on a continuous-time phase-domain delta–sigma modulator (PD$\Delta\Sigma$M), thus circumventing the kT/C noise limitations associated with SC readout circuits. To reduce the required dynamic range of the modulator, the large transients associated with the periodic heating pulses, and the offset associated with the baseline resistance of the resistive transducer are cancelled by employing two transducers in a novel bridge-type architecture. Experimental results show that the proposed CO_2 sensor achieves a resolution of 94 ppm in a conversion time of 1.8 s while dissipating only 12 mJ per measurement, or 2× more resolution than the state of the art [14], at an energy consumption that is >10× lower.

This paper is organized as follows. In Section II, the operation of steady-state TC sensing is first presented, followed by a discussion of transient TC sensing, as used in this paper. In addition, the principles of PD$\Delta\Sigma$M are briefly reviewed. Section III is devoted to the circuit implementation of the readout circuit, including the design of the PD$\Delta\Sigma$M and the techniques used to reduce its dynamic range requirements. Experimental results and discussions are presented in Section IV, and the conclusion is provided in Section V.

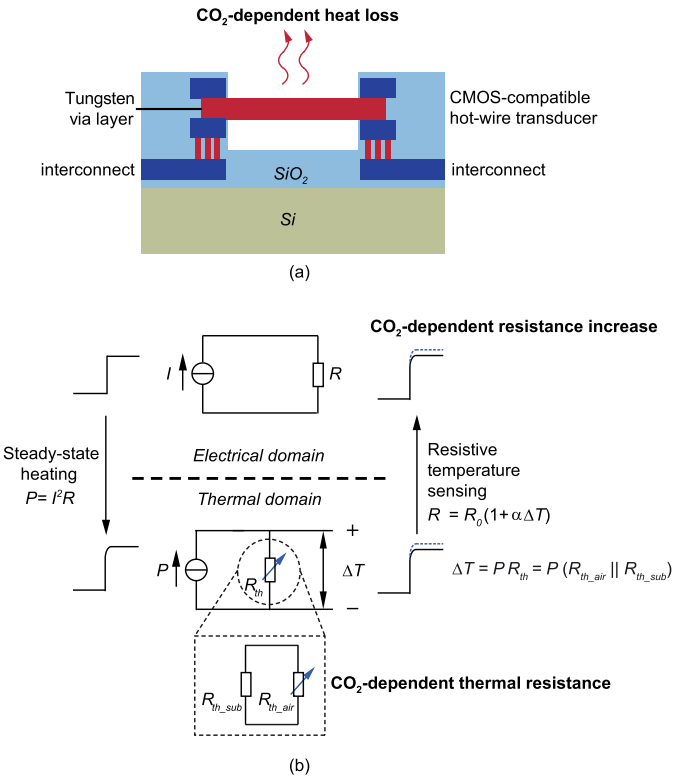

Fig. 1. (a) Cross-sectional view of the CO_2 transducer. (b) Steady-state TC (thermal resistance) measurement principle.

II. Operating Principle

A. Amplitude-Domain Thermal-Conductivity Sensing

Fig. 1(a) shows a cross section of the CMOS-compatible transducer used in this paper, which is the same as that reported in [14]. It consists of a suspended tungsten wire made in the via layer of the metal stack of a 0.16-μm CMOS process, which is released by means of a single etching step, using an approach similar to that described in [27]. As shown in Fig. 1(b), the temperature rise of the wire relative to ambient temperature (ΔT) caused by electrical power dissipation (P) is directly proportional to the equivalent thermal resistance R_{th} to ambient: the parallel combination of thermal resistance to the surrounding air ($R_{\text{th\_air}}$) and that to the substrate ($R_{\text{th\_sub}}$)

$$\Delta T = P \cdot R_{\text{th}} = P \cdot (R_{\text{th\_air}} \parallel R_{\text{th\_sub}}). \tag{1}$$

Since different gases have different TCs, $R_{\text{th\_air}}$ is a function of the air composition. The TC of CO_2 is slightly lower than the average TC of air, and thus a higher CO_2 concentration leads to a slightly higher temperature rise ΔT. Hence, ΔT can be used as a proxy for CO_2 concentration. To minimize the transducer's heat loss to the substrate, it is typically suspended above the substrate [14], [28], [29].

Resistance R of a hot-wire transducer can be approximated by a linear function of temperature T

$$R = R_0 \cdot (1 + \alpha \cdot (T - T_0)) \tag{2}$$

where α is the temperature coefficient of the electrical resistance of the transducer, and R_0 is its nominal value at

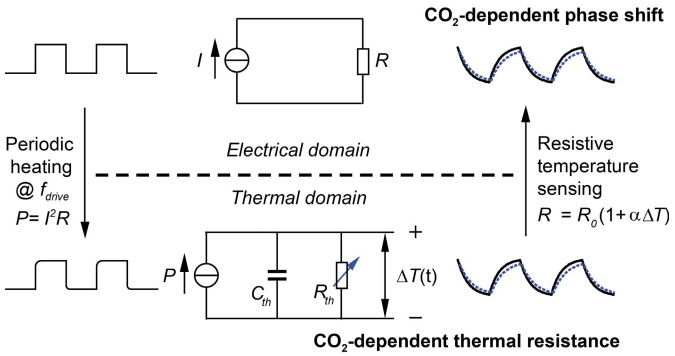

Fig. 2. Transient thermal-resistance (thermal delay) measurement principle.

temperature T_0. For our tungsten transducers, R_0 is 110 Ω, and α is 0.0017 /K (determined by experimental characterization of test devices). Thus, the temperature of the transducer can be measured via changes in its resistance [30], [31].

It is obvious that the accuracy of steady-state TC sensing depends on the accuracy with which the power dissipation P and the temperature rise ΔT (i.e., the temperature of the hotwire resistor relative to the ambient temperature) can be measured. Achieving less than 200-ppm error in the CO_2 concentration, corresponds to less than 80-ppm errors in TC, and therefore require similar levels of accuracy for both the measurement of P and ΔT [14]. Since this is well beyond the state of the art, it is very difficult to make integrated CMOS-compatible ambient CO_2 sensors based on steady-state TC sensing [14].

B. Time-Domain Thermal-Conductivity Sensing

Rather than measuring the steady-state temperature rise of a heated wire, an alternative method is to characterize its thermal time constant τ_{th}, which is the product of its thermal resistance to ambient (R_{th}) and its thermal capacitance (C_{th}) [15]–[17]. When the wire is driven with a current I_d pulsed at a frequency f_{drive}, and is thus periodically heated, its temperature transients are delayed relative to the driving pulses. The delay is determined by the thermal time constant τ_{th}, which in turn depends on the TC of the surrounding air (Fig. 2).

Such a TC sensor can be modeled as a first-order low-pass filter. Using a fixed driving frequency will then result in phase-delayed temperature transients relative to the driving pulses, from which τ_{th} can be derived. The optimal driving frequency equals the filter's pole frequency, i.e., $1/2\pi\,\tau_{\text{th}}$, at which the sensitivity of the phase shift to the changes of τ_{th} is maximal. For our devices, $\tau_{\text{th}} \approx 17\ \mu$s, leading to an optimal f_{drive} around 9–10 kHz.

Earlier TC sensors based on transient measurements employed separate resistive heaters and temperature sensors, either thermistors [16] or thermopiles [24], which were mounted together on a thermally isolated membrane. This separates the temperature transients from the electrical transients, and thus simplifies the readout circuitry, at the cost of fabrication complexity and hence cost.

In earlier work, sine waves [16] and square waves [24] have both been used to drive the heater. In terms of circuit implementation, a square wave is much easier to generate than a sine wave. The advantage of a sine wave is that it has no harmonics, and thus the phase shift of the temperature signal can be determined by filtering and zero-crossing detection [16]. In contrast, a square wave consists of a series of harmonics. The phase shift of the fundamental can then be detected by synchronous detection [24]. By employing a synchronous detector as the summing node of a delta–sigma modulator, a PDΔΣM can be realized with which the phase shift of the fundamental can be digitized with high resolution [32], [33].

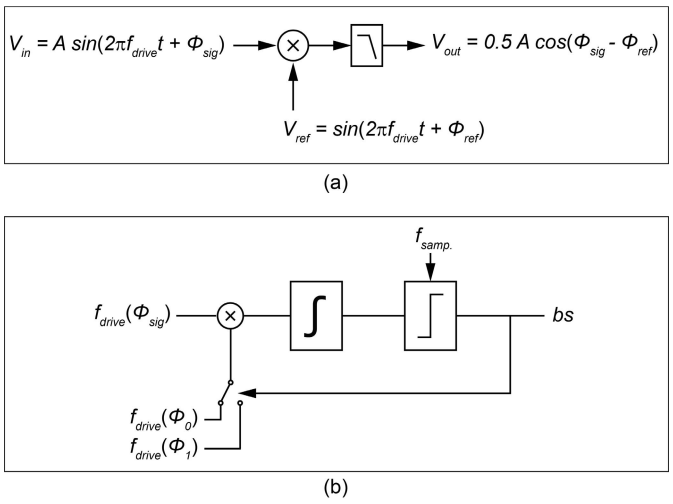

Fig. 3. (a) Phase detection by means of synchronous detection. (b) Phase detection using a delta–sigma feedback loop.

Since resistive transducers can be used both as a heater and a temperature sensor, the heating and sensing functions can, in principle, be combined in a single resistor, provided an appropriate readout scheme is devised. This will be discussed in Section III-A.

C. Phase-Domain Delta–Sigma Modulator

When driven at f_{drive}, the phase shift ϕ_{sig} of the transducer's temperature transients can be found by synchronous detection, i.e., by multiplying the transients by a reference signal at the same frequency and with a phase ϕ_{ref}, as illustrated in Fig. 3(a). Assuming sine waves for simplicity, the result is a dc component proportional to the cosine of the phase difference ($\phi_{\text{sig}} - \phi_{\text{ref}}$), and a component at $2f_{\text{drive}}$ that can be removed by a low-pass filter

$$A \cdot \sin(2\pi f_{\text{drive}} t + \phi_{\text{sig}}) \cdot \sin(2\pi f_{\text{drive}} t + \phi_{\text{ref}}) = 0.5 \cdot A \cdot \left[\cos(\phi_{\text{sig}} - \phi_{\text{ref}}) - \cos(4\pi f_{\text{drive}} t + \phi_{\text{sig}} + \phi_{\text{ref}})\right]. \quad (3)$$

As shown in Fig. 3(b), a PDΔΣM can be realized by embedding the synchronous detector in a delta–sigma (ΔΣ) loop [32], [33]. The loop's integrator serves as a low-pass filter and feedback is applied in the phase domain, by toggling ϕ_{ref} between two phase references ϕ_0 and ϕ_1 depending on the bitstream output bs. The feedback loop, on average, nulls the input of the integrator and thus ensures that the average

phase reference tracks the phase of the input signal, which can, therefore, be derived from the average value of the bitstream.

From (3) it can be seen that in order to allow the $\Delta\Sigma$ modulator to track ϕ_{sig}, the reference phase ϕ_{ref} should toggle between two values such that the polarity of the $\cos(\phi_{\text{sig}} - \phi_{\text{ref}})$ term also toggles. This implies that, with respect to the input signal, the two reference phases (ϕ_0 and ϕ_1) should be slightly less and slightly more than 90° (i.e., $\phi_0 = 90° + \Delta\phi/2$ and $\phi_1 = 90° - \Delta\phi/2$, where $\Delta\phi$ is the full scale of the PD$\Delta\Sigma$M). Given the relatively low frequency, such reference phases can be readily derived from a higher frequency master clock in practice.

The resolution with which the phase shift can be determined depends on the oversampling ratio (OSR), i.e., the number of clock cycles N that the $\Delta\Sigma$ modulator is operated per measurement, and equals $(\phi_1 - \phi_0)/N$ for a first-order $\Delta\Sigma$ modulator (given that the cosine non-linearity can be neglected over the relatively small range $\phi_1 - \phi_0$) [33].

Simulation shows that the phase shift induced by a 1-ppm change in CO_2 concentration is roughly 7 $\mu°$. The required OSR to arrive at the desired CO_2 resolution can thus be estimated from this. For example, for a full scale $\Delta\phi = \phi_0 - \phi_1 = 4°$, the required OSR for a quantization step equivalent to 100-ppm CO_2 is about 6000. Although this number could be reduced by using a second-order modulator, this would have little benefit in our design, because an even higher OSR is needed to reduce the thermal noise to the 100-ppm level, as will be shown in Section III-D. In designs in which the thermal-noise target can be reached at a lower OSR, increasing the order of the modulator could reduce the conversion time and thus result in less energy consumption per measurement.

III. Circuit Implementation

A. Front-End Dynamic Range Reduction Technique

While the voltage across the transducer in Fig. 2 contains temperature information, its sensitivity to temperature is proportional to the current level. As a result, the sensitivity will be much higher when the transducer is biased at the drive-current level to heat it up, than when it is biased at a lower current level. This complicates the extraction of the transducer's temperature transients from the voltage across it. To mitigate this, a small sense current I_s, switched at a much faster rate f_{sense}, produces a modulated voltage proportional to $R(t)$ with a sensitivity to temperature that is reasonably independent of the drive current [Fig. 4(a)].

To ease the detection of this voltage in the presence of the large voltage transients at f_{drive} (about 300-mV peak-to-peak), a pair of transducers are heated simultaneously by pulsed currents $I_d (= 2$ mA), and read out differentially via out-of-phase sense currents $I_s (= 0.5$ mA), switched at $f_{\text{sense}} = 15 \times f_{\text{drive}}$ [Fig. 4(b)]. Thus, the signal at f_{drive} is converted into a common-mode signal and can be rejected, while the differential signal is demodulated using a chopper switch, resulting in an output voltage V_s that contains the temperature transients at f_{drive}. Each transducer is also biased by an additional constant sense current $I_s (= 0.5$ mA) to

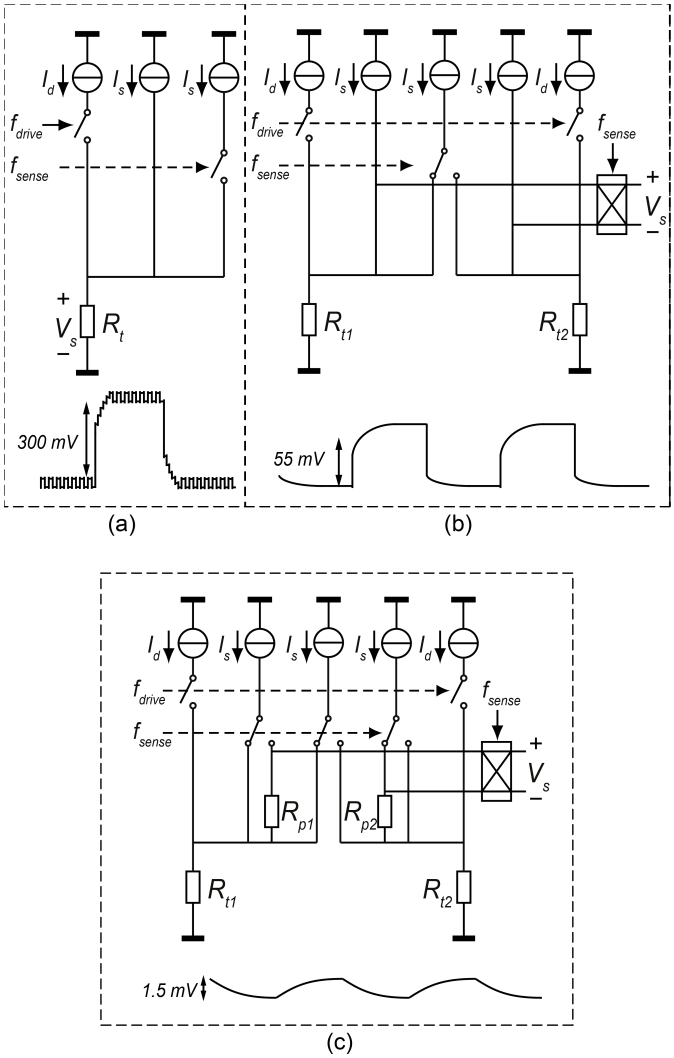

Fig. 4. Sensing the temperature-induced resistance changes using (a) current modulation, (b) differential sensing, and (c) baseline cancellation.

provide a voltage signal to be sensed when I_d is switched OFF. The sense current flowing through the transducers leads to a small baseline power dissipation that adds to the period heating due to the switching of I_d. For a given total average power dissipation, increasing the ratio I_d/I_s increases the amplitude of the temperature transients, and thus increases the signal to be sensed. At the same time, as will be detailed in Section III-D, a smaller value of I_s increases the noise level. The chosen 4:1 ratio between I_d and I_s is a tradeoff between these two effects and optimizes the SNR.

The ratio of 15 between f_{sense} and f_{drive} separates the drive and sense signals by more than a decade in the frequency spectrum, thus minimizing the thermal transients due to sense signal, and facilitating the filtering of the upconverted drive signal by the PD$\Delta\Sigma$M. An odd ratio is chosen to prevent errors due to the downconversion of harmonics of the drive signal. This is because any mismatch between the drive signals will cause a fraction of the common-mode drive signal to be converted into a differential-mode signal. If f_{sense} is an even multiple of f_{drive}, the odd harmonics of this differential-mode signal will be downconverted to f_{drive} by the chopper

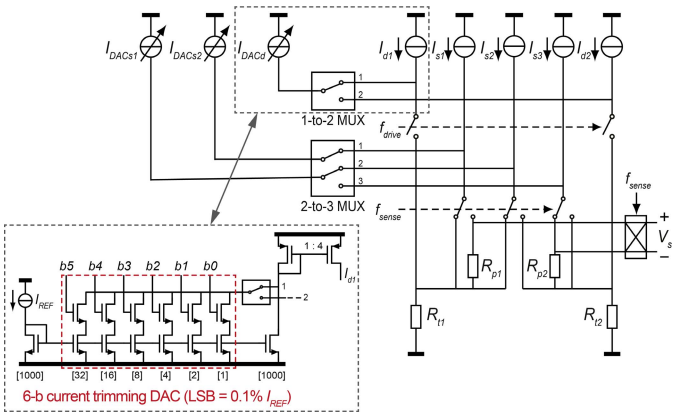

Fig. 5. Current trimming digital-to-analog converters to compensate for the mismatch between the resistive transducers as well as the poly-resistors. (One of the total three DACs is shown as example.)

demodulation at f_{sense}, and then detected by the PD$\Delta\Sigma$M, affecting the decimated results. If f_{sense} is chosen to be an odd multiple of f_{drive}, any downconverted harmonics will end up at dc, and will be rejected by the PD$\Delta\Sigma$M.

Even with this arrangement, a large dynamic range is still required, since the temperature-induced resistance increase ($\Delta R \approx 3\ \Omega$) is small compared to the baseline resistance ($R_0 = 110\ \Omega$), while the changes in ΔR due to changes in CO_2 concentration are even smaller (about 1.5 $\mu\Omega$ per ppm CO_2). To cancel the voltage steps associated with R_0, two poly-resistors $R_{p1,2}(= R_0)$ are connected in series with the transducers, and the sense currents are routed such that the additional voltage drop $I_s \cdot R_p$ cancels out $I_s \cdot R_0$ [Fig. 4(c)]. The remaining differential signal V_s is ideally equal to $I_s \cdot \Delta R$, and reflects the transient temperature change, which is about 1.5 mV, 200× smaller than the initial 300-mV transients.

Note that all switches in Fig. 4(c) are either in series with current sources or in voltage-sensing paths in which no significant current flows. As a result, the finite on-resistance of the switches, to first order, does not lead to measurement errors. The resistance of the interconnect between the transducers and the poly-resistors should be kept small compared to the nominal resistance of the transducers.

B. Current Trimming DACs

In practice, however, the mismatch between the transducers and the poly-resistors leads to ac ripple, which reduces the modulator's effective resolution and increases the requirements on its dynamic range. To minimize the ripple, three current digital-to-analog converters (DACs) are used to trim the drive and sense currents. As shown in Fig. 5, one 6-bit drive-current DAC (I_{DACd}, LSB $= 0.1\%I_{\text{REF}} = 0.025\%I_d$) is used to trim the two drive current sources and thus compensate for the mismatch between the two transducers R_{t1} and R_{t2}. Two 6-bit sense-current DACs (I_{DACs1} andI_{DACs2}, LSB $= 0.4\%I_s$) can be connected to two of the three sense current sources through a 2–3 multiplexer, to compensate for the mismatch between the two poly-resistors, and between the poly-resistors and the nominal resistance of the transducers.

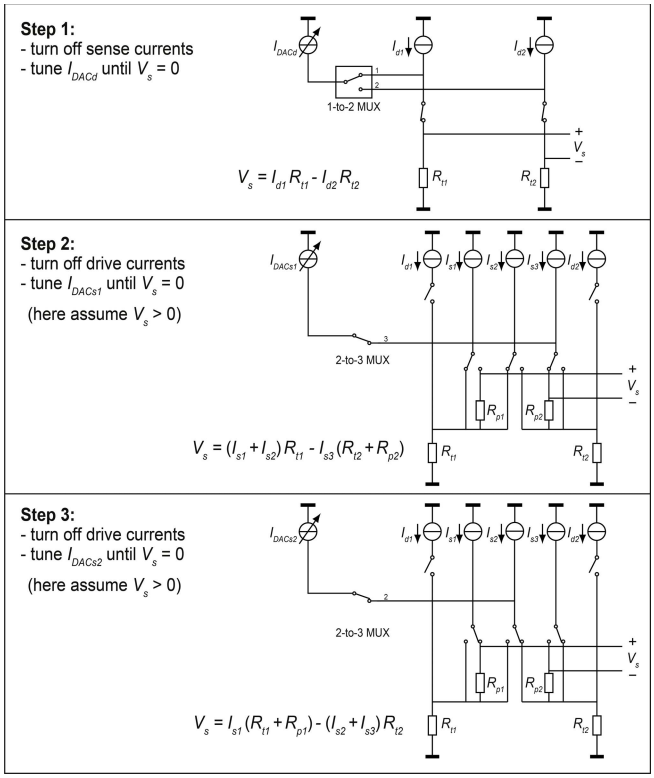

Fig. 6. Procedure to find the proper settings for the current trimming DACs.

If there would be no mismatch, the following would hold:

$$I_{d1}R_{t1} = I_{d2}R_{t2} \tag{4}$$

$$(I_{s1} + I_{s2})R_{t1} = I_{s3}(R_{t2} + R_{p2}) \tag{5}$$

$$I_{s1}(R_{t1} + R_{p1}) = (I_{s2} + I_{s3})R_{t2}. \tag{6}$$

Hence, the target of the current trimming is to configure the trimming DACs such that these conditions are reached.

The procedure used to find the proper trimming settings is shown in Fig. 6. First, only the two drive current sources are used to bias transducers R_{t1} and R_{t2}. The PD$\Delta\Sigma$M is disconnected and the voltage across V_s across the transducers is measured using an (off-chip) multimeter. Due to mismatch, V_s can be non-zero. The drive-current DAC is then used to compensate for this mismatch such that $V_s \approx 0$ and hence (4) holds. Second, only the sense current sources are switched on. When the switches are configured as shown, V_s is the voltage difference between the left and right branches, which ideally should be 0 as demonstrated by (5). Due to the variation of poly-resistor R_{p2}, this voltage can be above or below 0. Here, it is assumed that $V_s > 0$ as an example to demonstrate the trimming procedure. To reduce V_s to 0, I_{DACs1} is connected as shown to add current to I_{s3} and thus null V_s, so that (5) holds. Third, the switches for the sense current sources are changed to the other state. Again, due to mismatch, $V_s \neq 0$. Here, it is again assumed that $V_s > 0$. To reduce V_s to 0, I_{DACs2} is connected as shown to add current into I_{s2} and thus V_s, so that (6) holds.

In summary, current trimming is used to modify the sense currents I_{s1}, I_{s2}, and I_{s3} so as to compensate for the mismatch

of the resistors and drive the steady-state voltage difference between the left and right branches to 0. The example shown here is for $V_s > 0$ in both steps 2 and 3. For other cases, the proper settings of the DACs can be found in a similar way. By analyzing all possible cases, it is found that two multiplexed DACs for the three sense currents are sufficient, though three DACs may simplify the trimming procedure. To save die area, this design uses one trimming DAC for drive current and two trimming DACs for sense current.

The resolution of the trimming DACs is determined by the level of the residual ripple that the modulator can allow. An LSB of 0.4% of I_s current DAC can correct errors of resistance mismatch down to 0.4%, and the corresponding voltage ripple amplitude is about 0.2 mV, which is sufficiently small compared with the signal amplitude after baseline cancellation (1.5 mV). It should be noted that although this voltage ripple can increase the required dynamic range of the modulator and reduce the effective resolution, the relationship between the amplitude of the ripples and the CO_2 resolution is not straightforward.

The current trimming is done at room temperature, i.e., around the midpoint of the indoor temperature range (10 °C–40 °C). If the resistors only have mismatch in their baseline resistance but have the same temperature coefficient, the mismatch will be corrected by the current trimming, independent of further temperature variations. Mismatch in the temperature dependence of the resistance will lead to a (small) residual ripple that is larger for temperatures further away from the trimming temperature. Since the sensor operates over a very limited temperature range, we expect this residual ripple to be sufficiently small to avoid degrading the resolution.

C. Phase-Domain Delta–Sigma Modulator

The phase shift of the temperature-related differential signal $V_s(\approx I_s \cdot \Delta R)$ is digitized by a low-noise PD$\Delta\Sigma$M similar to that described in [25]. As shown in Fig. 7, before demodulation by f_{sense}, a low-noise transconductor g_m converts the differential voltage V_s into a current. This current passes through a chopper switch, which serves to dual purpose of demodulation by f_{sense} (like the chopper switch in Fig. 4), and multiplication with the phase-shifted versions of f_{drive} as a function of the bitstream [as shown in Fig. 3(b)]. This combination is realized by multiplying the phase-shifted versions of f_{drive} with f_{sense} by means of XOR gates. The resulting demodulated current is proportional to the phase difference between $V_s(t)$ and the selected phase reference. This difference is integrated on capacitors C_{int} of an active integrator and quantized using a clocked comparator, to form a $\Delta\Sigma$ loop which nulls the input of the integrator and thus ensures that the average phase reference tracks the phase of $V_s(t)$, which can, therefore, be derived from the average value of the bitstream.

To ensure that the noise from the transconductor is lower than that from the transducer and its bias circuit, g_m of the transconductor should be at least 400 μS. The transconductance of the g_m stage is about 560 μS. Fig. 8 shows the schematic of the g_m stage. It employs a gain-boosted folded-cascode structure for high output impedance to minimize

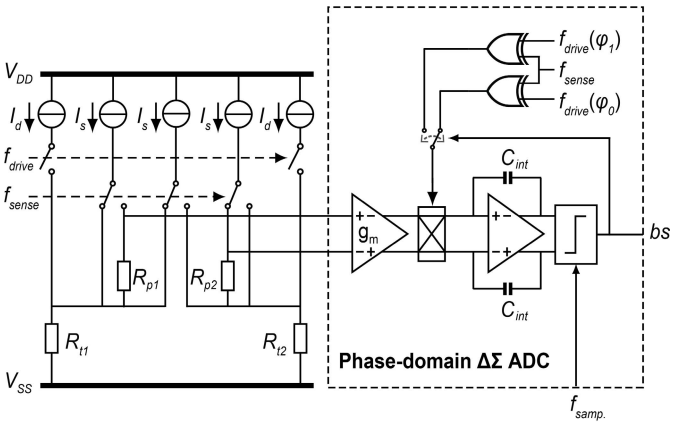

Fig. 7. Circuit diagram of the proposed readout circuit.

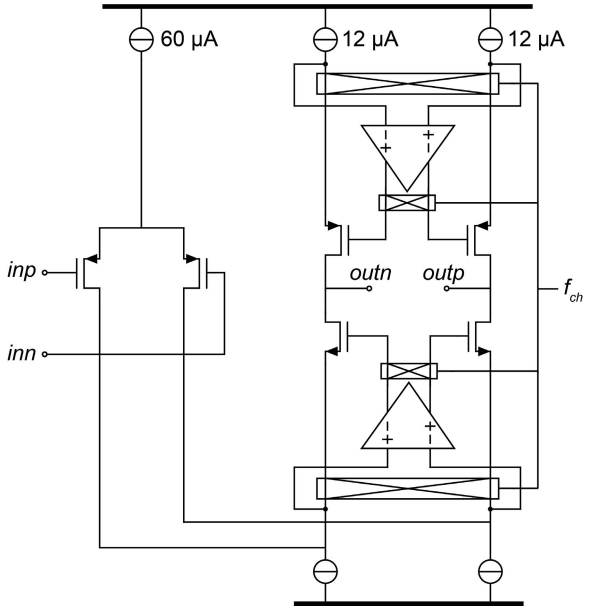

Fig. 8. Circuit diagram of transconductor with an embedded chopper demodulation.

the leakage of the integrator [25]. The chopper demodulator is embedded into the transconductor. The input pair of the transconductor is sized such that its $1/f$ noise corner frequency is below f_{sense}, ensuring that $1/f$ noise of the transconductor does not affect the measurement. The sampling frequency is chosen the same as f_{drive}. Both f_{drive} and f_{sense}, including the feedback signals at f_{drive} with reference phases ϕ_0 and ϕ_1, are derived from a single off-chip master clock. Capacitor C_{int} in the integrator is 50 pF.

D. Noise Analysis

The noise of the phase-domain $\Delta\Sigma$ analog-to-digital converter (ADC) can be analyzed using a charge-balancing analysis similar to that described in [34]. During a complete $\Delta\Sigma$ conversion, the total charge accumulated in the integrator is approximately 0. This includes all signal charge accumulated in the $\Delta\Sigma$ cycles when $bs = 0$ and when $bs = 1$, as well as the noise charge

$$Q_{\text{acc}} = Q_{\text{sig}} + q_{n,\text{acc}} = N[(1-\mu)Q_0 + \mu Q_1] + q_{n,\text{acc}} = 0 \tag{7}$$

in which Q_{sig} is the total signal charge and $q_{n,\text{acc}}$ is the total noise charge, N is the total number of $\Delta\Sigma$ cycles during one conversion, μ is the average value of the bitstream, Q_0 is the accumulated signal charge in one $\Delta\Sigma$ cycle when $bs = 0$, and Q_1 is the accumulated signal charge in one $\Delta\Sigma$ cycle when $bs = 1$.

Rearranging (7) results in the expression for μ

$$\mu = \frac{Q_0}{Q_0 - Q_1} + \frac{q_{n,\text{acc}}}{N(Q_0 - Q_1)} \tag{8}$$

in which the first part is the average value of the bitstream in the noise-free case, and the second part represents the noise contribution. The total accumulated noise charge is related to the noise charge q_n accumulated in one cycle as $q_{n,\text{acc}}^2 = N \cdot q_n^2$. By substituting this in (8), the standard deviation of μ can be expressed as

$$\sigma_\mu = \frac{1}{Q_0 - Q_1}\sqrt{\frac{q_n^2}{N}}. \tag{9}$$

Referring to Fig. 3, the signal charge difference $Q_0 - Q_1$ can be approximated as

$$\begin{aligned} Q_0 - Q_1 &= I_{\text{int}} \cdot t_{\text{clk}}[\cos(\phi_{\text{sig}} - \phi_0) - \cos(\phi_{\text{sig}} - \phi_1)] \\ &\approx I_{\text{int}} \cdot t_{\text{clk}}(\phi_0 - \phi_1) \end{aligned} \tag{10}$$

in which I_{int} is the output current of the transconductor g_m, t_{clk} is the inverse of the sampling frequency, and the approximation is justified as both $(\phi_{\text{sig}} - \phi_0)$ and $(\phi_{\text{sig}} - \phi_1)$ are close to $\pi/2$.

Noise charge accumulated in every cycle includes noise from the current source, the transducers, the transconductor g_m, and the chopper switches

$$q_n^2 = q_{n,cs}^2 + q_{n,Rt}^2 + q_{n,ch}^2 + q_{n,gm}^2 = 4kTR_n \cdot g_m^2 \cdot t_{\text{clk}}^2 \cdot B \tag{11}$$

in which $q_{n,cs}$ is the noise charge due to the current source, $q_{n,Rt}$ is the noise charge due to the transducers (including the poly-resistors), $q_{n,\text{ch}}$ is the noise charge generated by the chopper switches, $q_{n,gm}$ is the noise from the transconductor g_m, k is Boltzmann's constant, T is the absolute temperature, B is the equivalent noise bandwidth $(= 1/2t_{\text{clk}})$, and R_n is the equivalent noise resistance. The latter is given by

$$R_n = \gamma_1 g_{m,cs} R_t^2 + R_t + R_{\text{on,ch}} + \frac{\gamma_2}{g_m} \tag{12}$$

in which γ_1 and $g_{m,cs}$, are the excess noise factor and the transconductance of the current source, respectively, R_t is the resistance of the transducers, $R_{\text{on,ch}}$ is the on-resistance of the chopper switches, and γ_2 is the excess noise factor of the transconductor g_m. Substituting (10) and (11) into (9) results in an expression for the standard deviation of the output-referred noise

$$\begin{aligned} \sigma_\mu &= \frac{g_m}{I_{\text{int}}(\phi_0 - \phi_1)}\sqrt{\frac{2kTR_n}{N \cdot t_{\text{clk}}}} \\ &= \frac{16}{I_s \cdot \Delta R \cdot (\phi_0 - \phi_1)}\sqrt{\frac{2kTR_n}{N \cdot t_{\text{clk}}}} \end{aligned} \tag{13}$$

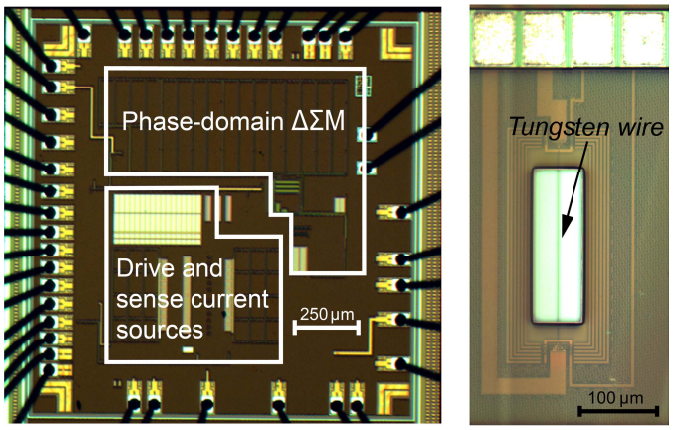

Fig. 9. Micrograph of the readout circuit and the transducer.

in which $I_{\text{int}} = (1/16)I_s \cdot \Delta R \cdot g_m$. Note that this derivation approximates the drive and sense currents, as well as the feedback signals as sinusoidal signals.

This expression shows that the standard deviation of μ and hence the resolution can be improved by decreasing the equivalent noise resistance, by increasing the total conversion time, or by increasing the signal amplitude $(I_s \cdot \Delta R)$. Note that the latter also requires an increase in the size of the integration capacitors, as the sampling frequency of the PD$\Delta\Sigma$M should not be higher than the drive frequency (f_{drive}). System-level simulations show that a 50-pF integration capacitor can handle a signal amplitude of about 1.5 mV. The resistance of the transducer is 110 Ω in this paper. We have chosen the drive current (2.5 mA) such that the temperature-induced resistance ΔR is limited to 3 Ω, and the sensing current I_s is 0.5 mA. The resulting calculated resolution, expressed in terms of an equivalent CO_2 concentration, is shown in Fig. 11 as a function of the number of $\Delta\Sigma$ cycles N (i.e., the OSR).

IV. Experimental Results and Discussion

Both the transducers and the readout circuit have been implemented in the same 0.16-μm CMOS technology (Fig. 9), with an active area of 0.3 and 3.14 mm^2, respectively. For flexibility, they have been realized on separate chips and connected on the PCB, and hence they can readily be co-integrated. When doing so, the impact of on-chip thermal gradients should be taken into account. Given that the hot-wire transducers lose the majority of their heat to the ambient air rather than to the substrate, and that the substrate is a good thermal conductor, we expect these gradients to be manageable. The readout circuit consumes 6.8 mW from a 1.8-V supply, a 6.3 mW of which is dissipated in the transducers.

All control signals, including f_{drive}, f_{sense}, the phase-shifted feedback reference signals, and control signals for the current DACs, are generated from a 10-MHz master clock using a field-programmable gate array (FPGA), and can be similarly generated on-chip in a future implementation. Jitter requirements for the clocks can be derived from the thermal time constant and required resolution. The transducer in this paper has a thermal time constant of about 17 μs.

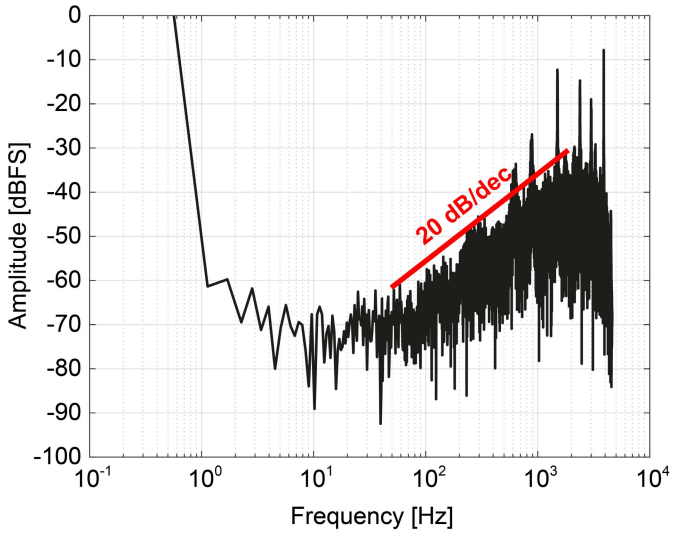

Fig. 10. Measured spectrum of the bitstream (FFT of 2^{14} points).

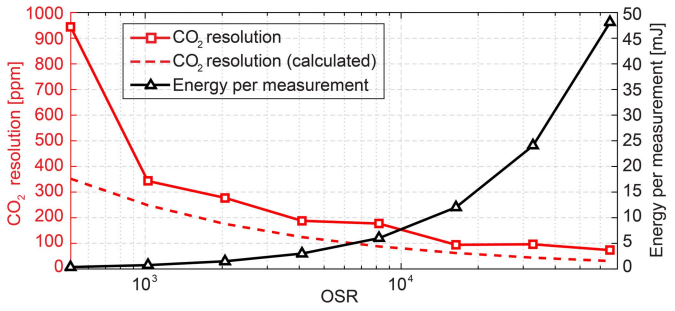

Fig. 11. Measured resolution (standard deviation of 20 consecutive measurements) and energy per measurement as a function of OSR.

A 100-ppm change in CO_2 corresponds to about 40-ppm change in TC, and so about 40-ppm change in thermal time constant ($\tau_{\text{th}} = R_{\text{th}}C_{\text{th}}$, and C_{th} is assumed to be constant), which is about 680 ps. To leave some margin, 100-ps jitter would be sufficient. The clock edges of f_{drive} and f_{sense} should be aligned to avoid possible mixing errors.

Fig. 10 shows the measured bitstream spectrum of the PD$\Delta\Sigma$M, demonstrating a first-order noise shaping similar to that of a conventional amplitude-domain first-order $\Delta\Sigma$ modulator. Note that the large amplitude in the first bin of the fast Fourier transform (FFT) is due to the non-zero dc value of the bitstream (which represents the phase shift to be digitized). The slightly sloped low-frequency noise could be due to $1/f$ noise of the current sources in the bias circuit.

Fig. 11 shows the measured resolution (standard deviation of 20 consecutive measurements) as well as corresponding energy per measurement at different oversampling ratios. The calculated CO_2 resolution (dashed curve) is derived from (13) and the measured sensitivity of decimated results to CO_2 concentration (1.6 ppm in μ per ppm CO_2). The measured resolution is in good agreement with the calculation in the thermal-noise-limited region where OSR $>$ 1000. At lower OSR, the performance is dominated by quantization errors. A resolution equivalent to 94-ppm CO_2 is reached at an OSR of 16 384, which corresponds to a measurement time of 1.8 s

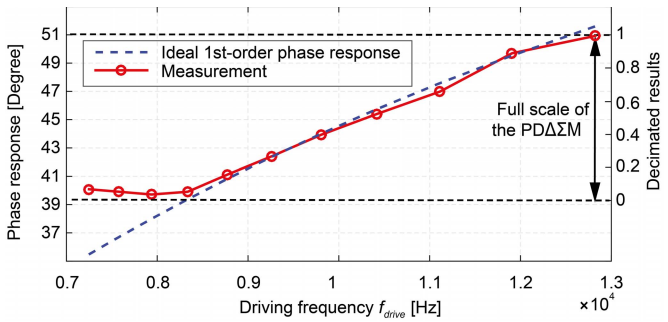

Fig. 12. Measured phase shift as a function of the drive frequency.

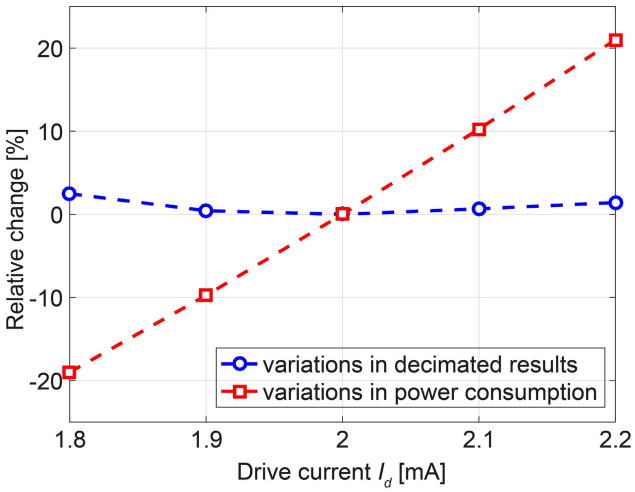

Fig. 13. Relative changes in the decimated results as well as in power consumption as a function of drive current.

($f_{\text{samp}} = f_{\text{drive}} = 9.26$ kHz), and an energy consumption of 12 mJ per measurement. This is a significant improvement compared with the amplitude-domain readout based on an SC integrator described in [14]. While the energy efficiency of the readout circuit in [14] could be further improved with some tradeoffs (i.e., by using larger sampling capacitors or a higher sampling rate), the continuous-time modulator used in this paper should still be better in terms of energy efficiency, as it avoids the inherent noise folding associated with SC circuitry.

The thermal delay, or equivalently the measured phase shift, caused by the thermal resistance and thermal capacitance, should present a first-order behavior as a function of the driving frequency, like a first-order electrical low-pass filter. This is confirmed by measurements, as shown in Fig. 12. The measured phase shift as a function of the drive frequency shows a good agreement with the ideal first-order behavior associated with the hot-wire's thermal time constant (measured using a larger full scale $\Delta\phi = \phi_0 - \phi_1 = 12^\circ$ for clarity).

To demonstrate the sensitivity of the sensor's output to variations in power consumption, Fig. 13 shows the decimated results and the power consumption as a function of the drive current I_d. With $\pm 10\%$ change in current, the power consumption changes by $\pm 20\%$, while the decimated results change by 2.5%, equivalent to a variation of about 1.5% in CO_2 concentration (given the sensitivity of 1.6 ppm per ppm CO_2). For 200-ppm accuracy in CO_2 measurement, this

TABLE I
PERFORMANCE SUMMARY AND BENCHMARKING

Parameter	This work	[14]	[16]	[5]	[8]
Method	TC	TC	TC	NDIR	NDIR
Technology	CMOS (0.16 μm)	CMOS (0.16 μm)	SOI MEMS	Module	SOI MEMS
Need for cross-sensitivity compensation	Y	Y	Y	N	N
On-chip readout	Y	Y	N	N	N
Area (sensor)	0.3 mm^2	0.6 mm^2	16 mm^2	-	†0.3 mm^2
Area (readout)	3 mm^2	3 mm^2	-	-	-
Supply voltage	1.8 V	1.8 V	-	5-14 V	-
Power consumption	††6.8 mW	††11.2 mW	††3 mW	200 mW	200 mW
Meas. time	1.8 s	30 s	60 s	2 s	2.4 s
CO_2 resolution	94 ppm	202 ppm	456 ppm	20 ppm	250 ppm
Energy / meas.	12 mJ	336 mJ	180 mJ	400 mJ	480 mJ

† Area of the IR emitter only, excluding 80-mm light tube and an infrared detector
†† Power consumption of the additional sensors (temperature, RH, pressure) for cross-sensitivity compensation is not included

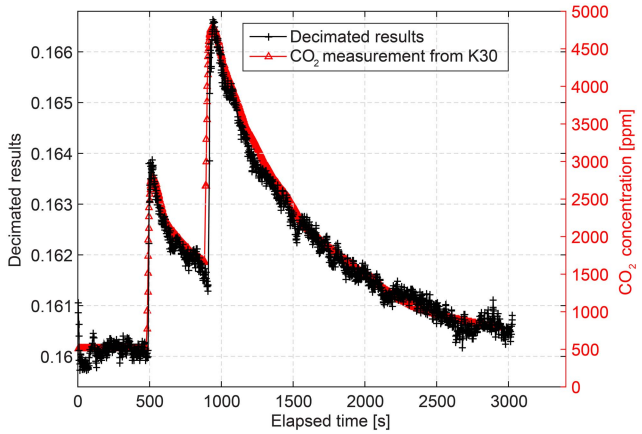

Fig. 14. Transient CO_2 response of the CO_2 sensor and an NDIR-based reference sensor (K30).

implies that variations in the power dissipation should be less than ±2600 ppm. Compared to the steady-state TC sensing, for which the required stability of the power dissipation would be <80 ppm when measuring in amplitude domain, the time-domain readout reduces the sensitivity to power level by 30–50×. The residual dependence could come from two possible sources. One is the temperature-dependent sensitivity [14]. Due to the change in power dissipation, the temperature of the hot-wire changes. It has been found in the previous work that the sensitivity of the TC of air to CO_2 concentration is not constant but temperature dependent. This could lead to power (temperature)-dependent measurement results. A second possible source of the residual current dependence is residual mismatch after trimming. This mismatch will appear as a dc input to the PDΔΣM, which causes ripple at the output of the integrator. Since the PDΔΣM has a finite ability to reject this ripple, and the amplitude of the ripple is proportional to the current level, the output of the PDΔΣM will depend on the current level.

To measure the CO_2 response, the sensor was placed in a sealed box along with an NDIR reference CO_2 sensor [5]. Like other TC-based sensors [14], [16], the sensor is cross-sensitive to ambient variations, such as temperature, humidity, and pressure, which therefore need to be compensated for in a final product. In our experiment, ambient temperature, humidity, and pressure sensors were placed in the sealed box to facilitate cross-sensitivity compensation. The results after compensation are shown in Fig. 14, demonstrating a good agreement between the readings of our sensor and the CO_2 concentration measured by the reference CO_2 sensor K30.

Table I summarizes the performance of the chip and compares it with the prior art. The proposed TC-based CO_2 sensor achieves a resolution of 94 ppm while dissipating only 12 mJ per measurement, which represents a significant improvement in energy efficiency compared to the state of the art for TC-based CO_2 sensors. Compared with the NDIR-based counterpart, the proposed sensor has advantages in cost (>10×) and volume (>100×) due to its CMOS-compatibility, and also consumes less energy. Implementation of on-chip cross-sensitivity compensation is future work, and remains essential for the realization of a practical TC-based CO_2 sensor. Several reported low-power, small-form-factor silicon sensors could be tailored for this application [35]–[37].

V. CONCLUSION

In this paper, we have presented a CMOS-compatible CO_2 sensor that senses the CO_2-dependent variations in the ambient air. Rather than measuring the steady-state temperature rise of a hot-wire transducer, we detect its thermal time constant τ_{th}, thus obviating the need for heating-power stabilization and accurate temperature sensing. The thermal time constant is the product of the wire's thermal capacitance and its thermal resistance to ambient, which in turn depends on the TC of the surrounding air. It is sensed by periodically heating up the wire and digitizing the phase shift in the resulting temperature transients by means of a low-noise PDΔΣM. The temperature transients are sensed through the resistance changes of the heater resistor, greatly simplifying the fabrication process compared to prior designs that employ separate resistive or thermopile-based temperature sensors closely integrated with the heater. In order to reduce energy consumption, the required dynamic range of the readout circuit is substantially reduced by cancelling the baseline resistance and by removing the impact of the large electrical driving signals. The sensor achieves a CO_2 resolution of 94 ppm at only 12-mJ energy consumption per measurement,

the best reported resolution in TC-based CO_2 sensors and the lowest energy consumption compared to the prior art. This makes this design a promising candidate for CO_2 sensing in cost- and energy-constrained applications.

ACKNOWLEDGMENT

The authors would like to thank L. Pakula and Z.-Y. Chang for their technical support.

REFERENCES

[1] *Standard Guide for Using Indoor Carbon Dioxide Concentrations to Evaluate Indoor Air Quality and Ventilation*, ASTM Int., West Conshohocken, PA, USA, Standard D6245–18, Jun. 2018.

[2] *Ventilation for Acceptable Indoor Air Quality*, ANSI/ASHRAE Standard 62.1, 2016.

[3] U. Satish *et al.*, "Is CO_2 an indoor pollutant? Direct effects of low-to-moderate CO_2 concentrations on human decision-making performance," *Environ. Health Perspect.*, vol. 120, no. 12, pp. 1671–1677, 2012.

[4] N. Nassif, "A robust CO_2-based demand-controlled ventilation control strategy for multi-zone HVAC systems," *Energy Buildings*, vol. 45, pp. 72–81, Feb. 2012.

[5] *SenseAir K30 Datasheet*. Accessed: Nov. 1, 2014. [Online]. Available: http://www.senseair.com/

[6] SGX Sensortech. *SGX Sensortech IR11BD Datasheet*. Accessed: Nov. 1, 2014. [Online]. Available: http://www.sgxsensortech.com/

[7] R. Frodl and T. Tille, "A high-precision NDIR CO_2 gas sensor for automotive applications," *IEEE Sensors J.*, vol. 6, no. 6, pp. 1697–1705, Dec. 2006.

[8] T. A. Vincent and J. W. Gardner, "A low cost MEMS based NDIR system for the monitoring of carbon dioxide in breath analysis at ppm levels," *Sens. Actuators B, Chem.*, vol. 236, pp. 954–964, Nov. 2016.

[9] S. Z. Ali, A. De Luca, R. Hopper, S. Boual, J. Gardner, and F. Udrea, "A low-power, low-cost infra-red emitter in CMOS technology," *IEEE Sensors J.*, vol. 15, no. 12, pp. 6775–6782, Dec. 2015.

[10] S. Z. Ali *et al.*, "Low power NDIR CO_2 sensor based on CMOS IR emitter for boiler applications," in *Proc. IEEE Sensors*, Nov. 2014, pp. 934–937.

[11] X. Chong, K. Kim, P. R. Ohodnicki, E. Li, C. Chang, and A. X. Wang, "Ultrashort near-infrared fiber-optic sensors for carbon dioxide detection," *IEEE Sensors J.*, vol. 15, no. 9, pp. 5327–5332, Sep. 2015.

[12] W.-Y. Chuang, C.-C. Wu, S.-S. Lu, and C.-T. Lin, "A printable conductive polymer CO_2 sensor with high selectivity to humidity," in *Proc. 19th Int. Conf. Solid-State Sens., Actuators Microsyst. (TRANSDUCERS)*, Jun. 2017, pp. 1501–1503.

[13] J. Boudaden, A. Klumpp, I. Eisele, and C. Kutter, "Smart capacitive CO_2 sensor," in *Proc. IEEE Sensors*, Oct. 2016, pp. 1–3.

[14] Z. Cai *et al.*, "A ratiometric readout circuit for thermal-conductivity-based resistive CO_2 sensors," *IEEE J. Solid-State Circuits*, vol. 51, no. 10, pp. 2463–2474, Oct. 2016.

[15] A. Mahdavifar, M. Navaei, P. J. Hesketh, M. Findlay, J. R. Stetter, and G. W. Hunter, "Transient thermal response of micro-thermal conductivity detector (μTCD) for the identification of gas mixtures: An ultra-fast and low power method," *Microsyst. Nanoeng.*, vol. 1, Oct. 2015, Art. no. 15025.

[16] K. Kliche, G. Kattinger, S. Billat, L. Shen, S. Messner, and R. Zengerle, "Sensor for thermal gas analysis based on micromachined silicon-microwires," *IEEE Sensors J.*, vol. 13, no. 7, pp. 2626–2635, Jul. 2013.

[17] K. Kliche, S. Billat, F. Hedrich, C. Ziegler, and R. Zengerle, "Sensor for gas analysis based on thermal conductivity, specific heat capacity and thermal diffusivity," in *Proc. IEEE Int. Conf. (MEMS)*, Jan. 2011, pp. 1189–1192.

[18] Xensor Integration. *XEN-5310 Datasheet*. Accessed: Sep. 1, 2017. [Online]. Available: http://www.xensor.nl/

[19] R. J. Heinsohn and J. M. Cimbala, *Indoor Air Quality Engineering: Environmental Health and Control of Indoor Pollutants*. New York, NY, USA: CRC Press, 2003.

[20] G. de Graaf and R. F. Wolffenbuttel, "Surface-micromachined thermal conductivity detectors for gas sensing," in *Proc. IEEE IIMTC*, May 2012, pp. 1861–1864.

[21] G. de Graaf, A. A. Prouza, M. Ghaderi, and R. F. Wolffenbuttel, "Micro thermal conductivity detector with flow compensation using a dual MEMS device," *Sens. Actuators A, Phys.*, vol. 249, pp. 186–198, Oct. 2016.

[22] Honeywell. *AWM5000 Datasheet*. Accessed: Sep. 1, 2017. [Online]. Available: https://sensing.honeywell.com/

[23] Z. Cai *et al.*, "A CMOS readout circuit for resistive transducers based on algorithmic resistance and power measurement," *IEEE Sensors J.*, vol. 17, no. 23, pp. 7917–7927, Dec. 2017.

[24] C. van Vroonhoven, G. de Graaf, and K. Makinwa, "Phase readout of thermal conductivity-based gas sensors," in *Proc. 4th IEEE Int. Workshop Adv. Sensors Interfaces (IWASI)*, Jun. 2011, pp. 199–202.

[25] S. M. Kashmiri, K. Souri, and K. A. A. Makinwa, "A scaled thermal-diffusivity-based 16 MHz frequency reference in 0.16 μm CMOS," *IEEE J. Solid-State Circuits*, vol. 47, no. 7, pp. 1535–1545, Jul. 2012.

[26] Z. Cai, R. van Veldhoven, H. Suy, G. de Graaf, K. A. A. Makinwa, and M. Pertijs, "A phase-domain readout circuit for a CMOS-compatible thermal-conductivity-based carbon dioxide sensor," in *ISSCC Dig. Techn. Papers*, Feb. 2018, pp. 332–334.

[27] M. Riverola, G. Vidal-Álvarez, G. Sobreviela, A. Uranga, F. Torres, and N. Barniol, "Dynamic properties of three-terminal tungsten CMOS-NEM relays under nonlinear tapping mode," *IEEE Sensors J.*, vol. 16, no. 13, pp. 5283–5291, Jul. 2016.

[28] I. Simon and M. Arndt, "Thermal and gas-sensing properties of a micromachined thermal conductivity sensor for the detection of hydrogen in automotive applications," *Sens. Actuators A, Phys.*, vols. 97–98, pp. 104–108, Apr. 2002.

[29] Z. Cai *et al.*, "An integrated carbon dioxide sensor based on ratiometric thermal-conductivity measurement," in *Proc. IEEE 18th Int. Conf. Solid-State Sens., Actuators Microsyst. (TRANSDUCERS)*, Jun. 2015, pp. 622–625.

[30] D. Ruffieux, F. Krummenacher, A. Pezous, and G. Spinola-Durante, "Silicon resonator based 3.2 μW real time clock with $\pm$10 ppm frequency accuracy," *IEEE J. Solid-State Circuits*, vol. 45, no. 1, pp. 224–234, Jan. 2010.

[31] S. Pan, Y. Luo, S. H. Shalmany, and K. A. A. Makinwa, "A resistor-based temperature sensor with a 0.13 pJ·K2 resolution FoM," *IEEE J. Solid-State Circuits*, vol. 53, no. 1, pp. 164–173, Jan. 2018.

[32] C. P. L. van Vroonhoven and K. A. A. Makinwa, "A thermal-diffusivity-based temperature sensor with an untrimmed inaccuracy of $\pm$0.2°c (3s) from -55°c to 125°c," in *IEEE Int. Solid-State Circuits Conf. (ISSCC) Dig. Techn. Papers*, Feb. 2010, pp. 314–315.

[33] S. M. Kashmiri, S. Xia, and K. A. A. Makinwa, "A temperature-to-digital converter based on an optimized electrothermal filter," *IEEE J. Solid-State Circuits*, vol. 44, no. 7, pp. 2026–2035, Jul. 2009.

[34] M. A. P. Pertijs and J. Huijsing, *Precision Temperature Sensors in CMOS Technology*. Dordrecht, The Netherlands: Springer-Verlag, 2006.

[35] B. Yousefzadeh, S. Heidary Shalmany, and K. A. A. Makinwa, "A BJT-based temperature-to-digital converter with $\pm$60 mK (3σ) inaccuracy from -55 °C to $+125$ °C in 0.16-μm CMOS," *IEEE J. Solid-State Circuits*, vol. 52, no. 4, pp. 1044–1052, Apr. 2017.

[36] Z. Tan, R. Daamen, A. Humbert, Y. V. Ponomarev, Y. Chae, and M. A. P. Pertijs, "A 1.2-V 8.3-nJ CMOS humidity sensor for RFID applications," *IEEE J. Solid-State Circuits*, vol. 48, no. 10, pp. 2469–2477, Oct. 2013.

[37] S. Oh *et al.*, "A dual-slope capacitance-to-digital converter integrated in an implantable pressure-sensing system," *IEEE J. Solid-State Circuits*, vol. 50, no. 7, pp. 1581–1591, Jul. 2015.

Zeyu Cai (S'15–M'16) received the B.Eng. degree in communication engineering from Nankai University, Tianjin, China, in 2004, and the M.Sc. degree (with distinction) in electronics: analog system design from The University of Edinburgh, Edinburgh, U.K., in 2011. He is currently pursuing the Ph.D. degree with the Electronic Instrumentation Laboratory, Delft University of Technology, Delft, The Netherlands, with a focus on low-cost, low-power CMOS-compatible carbon dioxide sensors for next-generation home and building automation systems.

From 2005 to 2010, he was a Product Engineer with Qorvo, Inc., Beijing, China. Since 2017, he has been a Senior Analog Design Engineer with the Personal Health Group, NXP Semiconductors, Eindhoven, The Netherlands. His current research interests include precision analog circuits, low-power delta–sigma ADCs, and energy-efficient sensor interfaces.

Mr. Cai serves as a Reviewer for peer-reviewed journals, including the IEEE TRANSACTIONS ON CIRCUITS AND SYSTEMS I (TCAS-I), the *Electronics Letters*, and the IEEE SENSORS JOURNAL.

Robert van Veldhoven (SM'12) was born in Eindhoven, The Netherlands, in 1972. He received the Ph.D. degree in electrical engineering from the University of Eindhoven, Eindhoven.

In 1996, he joined Philips Research, and moved to NXP, Eindhoven, The Netherlands, in 2006. He has authored or co-authored over 15 ISSCC/JSSC papers. He holds over 25 U.S. patents. His current research interests include data converters and sensors.

Dr. van Veldhoven is a reviewer for several professional journals and conferences. From 2004 to 2010, he was invited to give an ISSCC forum presentation on $\Sigma\Delta$ modulators for wireless and cellular receivers.

Hilco Suy received the M.Sc. degree (*cum laude*) in mechanical engineering from the Eindhoven University of Technology, Eindhoven, The Netherlands, in 2005.

In 2005, he joined Philips Research and moved into NXP in 2006, where he started his work on capacitive and galvanic MEMS switches. From 2009 to 2012, he worked on capacitive biosensors in a microfluidic system, among others also under the scope of the ENIAC Project CAJAL4EU. Since 2012, he has been working on environmental sensors, such as gas, temperature, relative humidity, and pressure sensors. The NXP sensor business was acquired by ams-AG in 2015, where he has continued his research in this field. His current research interests include MEMS, sensors, multiphysics modeling and test, and calibration of MEMS.

Ger de Graaf received the Ph.D. degree from Delft University of Technology, Delft, The Netherlands, with a focus on MEMS infrared spectrometers, in 2008.

He is a Staff Member with the Faculty of Electrical Engineering, Delft University of Technology. He is currently working on sensors for composition detection in gases, in bioprocesses, and in fuel. His current research interests include MEMS, analog electronic design, sensors and actuators, and microfabrication in general.

Kofi A. A. Makinwa (M'97–SM'05–F'11) received the B.Sc. and M.Sc. degrees from Obafemi Awolowo University, Ife, Nigeria, in 1985 and 1988, respectively, the M.E.E. degree from the Philips International Institute, Eindhoven, The Netherlands, in 1989, and the Ph.D. degree from the Delft University of Technology, Delft, The Netherlands, in 2004.

From 1989 to 1999, he was a Research Scientist with the Philips Research Laboratories, Eindhoven, where he worked on interactive displays and digital recording systems. In 1999, he joined the Delft University of Technology, where he is currently an Antoni van Leeuwenhoek Professor and the Head of the Microelectronics Department. He has co-authored over 15 books and over 250 technical papers, and holds 26 patents. His current research interests include the design of mixed-signal circuits, sensor interfaces, and smart sensors.

Dr. Makinwa is a member of the Royal Netherlands Academy of Arts and Sciences and a member of the Editorial Board of the PROCEEDINGS OF THE IEEE. He was a co-recipient of 15 best paper awards from the JOURNAL OF SOLID-STATE CIRCUITS (JSSC), International Solid-State Circuits Conference (ISSCC), very large scale integration (VLSI), European Solid-State Circuits Conference (ESSCIRC), and Transducers. He received the 2005 Simon Stevin Gezel Award from the Dutch Technology Foundation. At the 60th anniversary of ISSCC, he was recognized as a top-10 contributor. He is currently the Analog Subcommittee Chair of the ISSCC. He is also on the program committees of the VLSI Symposium, the ESSCIRC, and the Advances in Analog Circuit Design (AACD) Workshop. He is a Guest Editor of the IEEEJSSC. He served as a Distinguished Lecturer and an Elected AdCom Member for the IEEE Solid-State Circuits Society.

Michiel A. P. Pertijs (S'99–M'06–SM'10) received the M.Sc. and Ph.D. degrees (*cum laude)*in electrical engineering from the Delft University of Technology, Delft, The Netherlands, in 2000 and 2005, respectively.

From 2005 to 2008, he was with National Semiconductor, Delft, where he designed precision operational amplifiers and instrumentation amplifiers. From 2008 to 2009, he was a Senior Researcher with imec/Holst Centre, Eindhoven, The Netherlands. In 2009, he joined the Electronic Instrumentation Laboratory, Delft University of Technology, where he is currently an Associate Professor. He is currently the Head of the research group focusing on integrated circuits for medical ultrasound and energy-efficient smart sensors. He has authored or co-authored over two books, three book chapters, 12 patents, and over 90 technical papers.

Dr. Pertijs is a member of the Technical Program Committee the European Solid-State Circuits Conference (ESSCIRC). He was a recipient of the International Solid-State Circuits Conference (ISSCC) 2005 Jack Kilby Award for Outstanding Student Paper and theJOURNAL OF SOLID-STATE CIRCUITS (JSSC) 2005 Best Paper Award. For his Ph.D. research on high-accuracy CMOS smart temperature sensors, he received the 2006 Simon Stevin Gezel Award from the Dutch Technology Foundation STW. He served as an Associate Editor for the IEEE JSSC, and also served on the program committees for the International Solid-State Circuits Conference and the IEEE Sensors Conference. In 2014, he was elected Best Teacher of the EE Program at the Delft University of Technology.